AGU PUBLICATIONS

JGR

Journal of Geophysical Research: Oceans

RESEARCH ARTICLE

10.1002/2014JC009969

Special Section:

Early scientific results from the salinity measuring satellites Aquarius/SAC-D and SMOS

Key Points:

- Aquarius SSS shows regions of strong seasonal SSS variability
- Different dynamics controlling regional variability are identified
- Identified dynamics and salinity stratifications are discussed

Correspondence to:

J.-H. Moon,
Jae-Hong.Moon@jpl.nasa.gov

Citation:

Moon, J.-H., and Y. T. Song (2014), Seasonal salinity stratifications in the near-surface layer from Aquarius, Argo, and an ocean model: Focusing on the tropical Atlantic/Indian Oceans, *J. Geophys. Res. Oceans*, *119*, 6066–6077, doi:10.1002/2014JC009969.

Received 13 MAR 2014
Accepted 22 AUG 2014
Accepted article online 26 AUG 2014
Published online 15 SEP 2014

Seasonal salinity stratifications in the near-surface layer from Aquarius, Argo, and an ocean model: Focusing on the tropical Atlantic/Indian Oceans

Jae-Hong Moon[1] and Y. Tony Song[1]

[1]Jet Propulsion Laboratory, California Institute of Technology, Pasadena, California, USA

Abstract A newly available sea surface salinity (SSS) measurement from Aquarius/SAC-D satellite reveals strong seasonal variability in the tropical Atlantic and Indian Oceans. The seasonal SSS variability at skin layer differs/agrees regionally in their amplitude from/with Argo-measured salinity at 5 m depth and model salinity at the top layer, indicating various characteristics of near-surface salinity stratifications. By comparing the three different salinity products, we have examined the near-surface salinity stratifications with emphasis on the dynamical processes that differ from one region to another. Our analysis shows that for the western part of tropical Atlantic and southern tropical Indian, a large amount of river runoff and/or surface freshwater significantly stratifies the surface layer above 5 m depth, resulting in the differences among the Aquarius, Argo, and model. Differently for the southern Arabian Sea, the surface water can be mixed down to the depth of 5 m due to seasonally reversing currents driven by monsoons, resulting in an agreement among the data sets. The comparison suggests that dynamical differences can lead to different vertical salinity stratifications locally, which explain the differences between the Aquarius observations in the first cm of the sea surface, the Argo measurements at the 5 m depth, and model's representation of the surface-layer averaged salinity.

1. Introduction

Sea surface salinity (SSS) is an important factor contributing to changes in the global hydrological budget, and its spatial and temporal distributions are essential to improve understanding of the hydrological cycle and oceanic processes, such as mixing, water mass formation, and circulations [*Yu*, 2011]. Unlike sea surface temperature available from remote sensing, in situ SSS data are relatively sparse and have been heavily smoothed in space and time although recent Argo floats improved the availability of in situ measurement [*Roemmich and Gilson*, 2009]. Since launched in November 2009, the Soil Moisture and Ocean Salinity (SMOS) mission from the European Space Agency opened a new era for observing and monitoring SSS field. The SMOS and more recent Aquarius/Satélite de Aplicaciones Científicas (SAC)-D missions, which is a collaborative effort between NASA and the Argentinian Space Agency Comision Nacional de Actividades Espaciales (CONAE), are providing the first ever spatially complete global SSS (a few cm of ocean surface) field. Both satellite missions have already shown many features of SSS structure including the near-surface barrier layer variability in the equatorial Pacific [*Qu et al*., 2014], intensification of hurricanes to the presence of Amazon plume [*Grodsky et al*., 2012], surface freshening due to heavy rains [*Boutin et al*., 2013], and salinity variability and horizontal salt flux in the tropical Atlantic [*Tzortzi et al*., 2013; *Grodsky et al*., 2014a, 2014b].

So far, many previous studies on SSS variability have relied on irregularly distributed and heavily interpolated climatological data sets and Argo measurements. Furthermore, climatological and typical Argo SSS are taken at several meters depth, which are different from the true SSS inferred from in situ measurement (at about 5 m depth). On the other hand, the two satellites measure the salinity at the first centimeter or skin layer of the sea surface, which can be significantly different from a typical top level of around 5 m depth by Argo. Preliminary studies based on Argo vertical profiles and ship measurements have shown the vertical salinity differences between 1 and 10 m depth [*Henocq et al*., 2010; *Boutin et al*., 2013]. *Henocq et al*. [2010] reported that in situ salinity measurement between 1 and 10 m depth differs by 0.1–0.5 psu in rainy regions. *Boutin et al*. [2013] focused on the impact of rain on the surface freshening relative to Argo, which reflects surface vertical stratification. This issue of uppermost salinity stratification is getting more and more attention in recent years because recent two satellites are providing a skin value within 1 cm of the surface that will complement in situ measurements and help to better understand the near-surface salinity variability and SSS-related processes at global and local scales. In this study, we compare the newly available Aquarius SSS with the Argo floats and an ocean circulation model to examine the different surface vertical salinity stratifications locally and their dynamical differences.

The Aquarius/SAC-D mission has now released two full years of SSS data from September 2011 to October 2013. As a case study, we here focused on annual near-surface salinity variability in the tropical Atlantic/Indian Oceans. To estimate the contribution of air-sea flux to the SSS change, we also analyzed the precipitation (P) and evaporation (E) data from NCEP reanalysis products, the satellite-gauge product of the Global Precipitation Climatology Project (GPCP) [*Huffman and Bolvin*, 2012], and the Objectively Analyzed air-sea Fluxes (OAFlux), which is a combination of satellite and reanalysis data [*Yu et al.*, 2008].

The observational data and model descriptions are given in section 2, while characteristics of the tropical Atlantic/Indian Oceans are reviewed in section 3. In sections 4 and 5, we compare Aquarius-derived seasonal SSS with Argo measurements and model results and then discuss an interpretation in terms of the SSS differences among the products, which may be associated with regional ocean dynamics. A summary and discussions are provided in section 6.

2. Data and Model Descriptions

2.1. Aquarius Data

Aquarius/SAC-D collects data in 386 km swaths in an orbit designed to obtain a complete survey of global SSS of ice-free ocean every 7 days. Since its launch in June 2011, the Aquarius is providing global SSS maps at monthly 150 km resolution and 0.2 psu accuracy over the mission lifetime [*Lagerloef et al.*, 2008, 2013]. We use monthly mean SSS products (Level-3) at $1^\circ \times 1^\circ$ spatial resolution from the Aquarius/SAC-D version 2.5 data, which is almost the same as the version 3.0 that will be released soon. The retrieved SSS data for ascending and descending tracks were bias adjusted on monthly time scale, and the global salinity root-mean-square error is no more than 0.2 psu on 150×150 km and monthly average. The Aquarius salinity sensor detects the microwave emissivity in the top few centimeter of ocean water. Since this study focuses on the large-scale seasonal variability associated with ocean dynamics rather than the assessment through the point-by-point comparison, we here use the 1° resolution gridded Aquarius data. The data from Argo and model also have been gridded into the same 1° map of Aquarius to directly compare the seasonal variability. For all data sets, we used the monthly averaged SSS for the same month in different years to minimize the impact of seasonal errors which will be discussed in section 4.

2.2. Argo SSS

Argo is a global array of profiling floats measuring temperature and salinity in upper 2000 m of the ocean. After 10 days of repeat cycle, the floats come up to the surface to transmit data to a satellite. Although there are still many areas yet to be sampled, the Argo floats are one of the main sources of in situ salinity measurements. The Argo measurements extend from a typical surface around 5–2000 m depth. More than 3500 of Argo floats are currently distributed globally and a near-real time, monthly product at a $1^\circ \times 1^\circ$ grid is recently created by the Asian Pacific Data Research Center of the International Pacific Research Center, University of Hawaii (data available at http://apdrc.soest.hawaii.edu/dods/public_data/Argo_Products/monthly_mean). This product has 26 standard levels in the upper 2000 m, and a variational analysis was used to interpolate temperature and salinity onto a 3-D spatial grid [*Qu et al.*, 2014]. This gridded Argo near-surface ($\sim$5 m depth) salinity data are used as a proxy for SSS in the Atlantic and Indian Oceans during the period from September 2011 to September 2013.

2.3. Ocean Circulation Model

We here use the global non-Boussinesq ROMS based on *Song and Hou* [2006], which is an evolving version of ROMS [*Shchepetkin and McWilliams*, 2005]. The model has been configured globally with a 1/4° horizontal resolution with 30 terrain-following vertical levels [*Song and Haidvogel*, 1994] and is coupled with a sea ice model [*Budgell*, 2005]. The shallowest and deepest water depths are 20 and 5500 m, respectively. The model was spun up for 60 years with National Centers for Environmental Prediction (NECP)/National Center for Atmospheric Research (NCAR) monthly climatology [*Kalnay et al.*, 1996] to reach an approximately steady

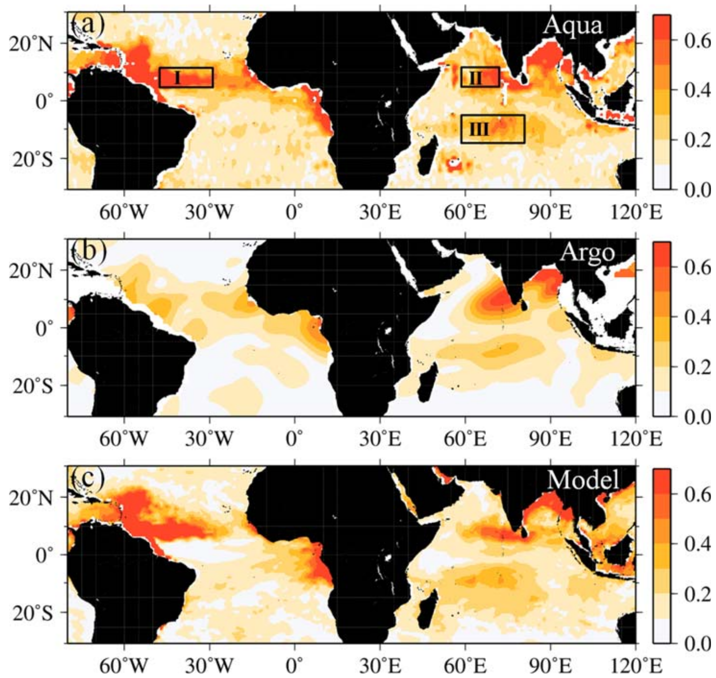

Figure 1. Annual amplitude maps of sea surface salinity (SSS) from (a) Aquarius, (b) Argo, and (c) model. Three selected regions, I: the western part of tropical Atlantic, II: the southern Arabian Sea (AS), III: the southern tropical Indian, indicate the areas where the seasonal variability will be examined.

state. After 60 years spin-up, the model was forced by six-hourly NCEP/NCAR reanalysis data from 1958 to 2013. Surface fluxes of momentum and heat are calculated in ROMS using bulk formulations [*Fairall et al.*, 1996]. Salt flux in the model is basically balanced by P and E, which is corrected by SSS climatology with 90 days relaxation time. Monthly averaged results for the same month during September 2011 to September 2013 were used to compare with the Aquarius and Argo measurements and to explain the dynamics of seasonal SSS variability in the tropical Atlantic/Indian Oceans.

3. Study Regions: Tropical Atlantic/Indian Oceans

The annual amplitudes of SSS for the three products are shown in Figure 1, which compares their spatial pattern in the Atlantic/Indian Oceans. Most of the oceans have annual amplitudes of SSS less than 0.2 psu, but relatively strong variations are shown in the tropical regions. Overall, the Aquarius and model show a similar variability of SSS in amplitude and spatial pattern. However, the Argo SSS has the smallest variability in amplitude except for the southern region of Arabian Sea (AS) although the spatial pattern is quite similar to those of Aquarius and model.

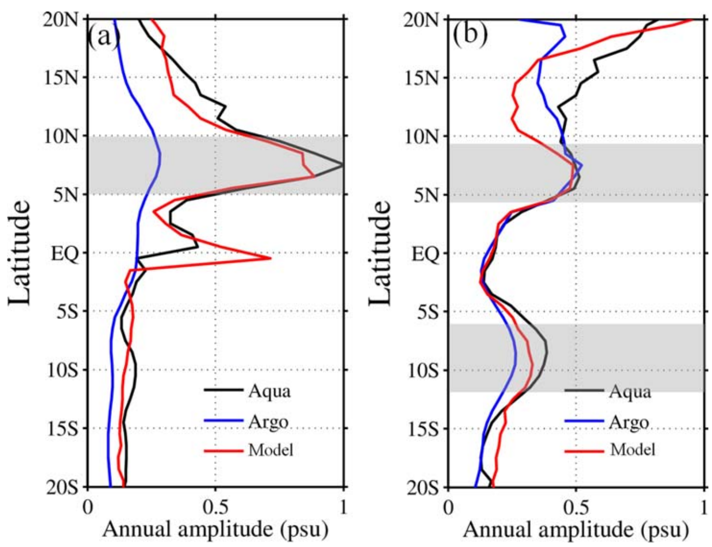

Figure 2. Zonally averaged seasonal SSS amplitudes for the three products of Aquarius (black), Argo (blue), and model (red) in (a) Atlantic Ocean and (b) Indian Ocean. The shaded regions indicate the zones where the Aquarius differences of annual amplitude from Argo are relatively large.

In the Atlantic Ocean, the strongest SSS variability is found along 5°N–10°N band (marked by Region I in Figure 1a, 50°W–30°W, 5°N–10°N) in Aquarius, with the largest difference from the Argo (Figure 1b). The model result is closer to the variability of Aquarius SSS than to the Argo. This feature is also shown in Figure 2a that compares the zonally averaged annual amplitudes of SSS in the tropical Atlantic Ocean, emphasizing the strongest difference between the Aquarius and Argo along 5°N–10°N band (marked by shaded region). This region is known to be characterized by low SSS and off major rivers, such as Amazon/Orinoco and Congo [e.g., *Foltz and McPhaden*, 2008; *Tzortzi et al*., 2013]. It is also known that the SSS variability is governed by several processes including changes in freshwater outflow from the Amazon River, horizontal advection, and mixing by strong winds in the tropical region [*Hu et al*., 2004; *Nikiemaa et al*., 2007; *Da-Allada et al*., 2013]. In particular, horizontal advection by North Equatorial Counter Current (NECC) mainly contributes to seasonal SSS variability in the western tropical region [*Grodsky et al*., 2014b]. During summer to fall, low-salinity water discharged from the Amazon River is transported eastward by NECC after flowing northward along the North Brazil Current (NBC) in the shelf region.

In the Indian Ocean, annual amplitude maps of SSS for the three products show three significant features (see Figure 1). The first feature is along the coastal regions of Bay of Bengal (BOB), where the excess P and river runoff stratify the sea surface layer [*Donguy and Meyers*, 1996; *Rao and Sivakumar*, 2003; *Schott and McCreary*, 2001; *Ravichandran et al*., 2004; *Delcroix et al*., 2005]. The second is in the southern AS region centered at about 6°N (marked by Region II, 60°W–72°W, 5°N–10°N) that shows a strong seasonal SSS variability for all products. The AS is characterized by high-saline surface water due to excess of E over P. The AS and the BOB communicate with each other through seasonal current system driven by monsoon winds [*Delcroix et al*., 2005; *Subrahmanyam et al*., 2011]. The third is a zonal band structure in the southern tropical region centered along 8°S (marked by Region III, 60°W–80°W, 5°S–12°S), with the largest amplitude in Aquarius. These features are also represented in Figure 2b, showing the strong annual amplitudes along about 8°S, 6°N zones, and at midlatitude (above 15°N). The largest difference from the Argo takes place at midlatitude (i.e., coastal regions of BOB), which may be associated with the land contamination in the satellite footprint. The other large difference in annual SSS amplitude is found along the southern tropical region, coinciding with the Intertropical Convergence Zone (ITCZ). *Nyadjro et al*. [2010] mentioned that this region could be linked to the dynamics of the ITCZ and the pathway of the Indonesian Throughflow (ITF). To quantify and directly compare the seasonal variability among the three SSS products, in this study, we focus on the tropical Atlantic and Indian Oceans, where the strong amplitudes of seasonal SSS variation are found, and selected the three regions away from coastal boundaries (marked I, II, and III in Figure 1a) to avoid possible land contaminations (e.g., low-level radio frequency interference for Aquarius and insufficient samplings for Argo). Therefore, the comparison for coastal regions around Amazon River, Congo River, and BOB are not considered in this paper.

4. Comparison of Seasonal SSS Variability

The 2 year mean variations of averaged SSS deviations over the three regions show a remarkable seasonal variability (Figure 3). For Aquarius data, the strongest SSS variability is seen in the western part of tropical Atlantic, Region I, with its maximum in March and minimum in September (Figure 3a). A fresh signature begins to appear from the west of Region I, and then is transported to the east during June to November (Figure 4a). This seasonal change may closely depend on river discharge from Amazon accounting for approximately one-fifth of the world's total river flow. On the other hand, the southern AS, Region II, has an opposite phase signal to the Region I (Figure 3b), showing that freshwater comes from the east and then is transported to the west during winter-spring (Figure 4d). The strong annual cycle in this region may be linked to the seasonally reversing ocean currents driven by monsoon wind. Region III exhibits the same annual cycle as the Region II, with relatively smaller amplitude than those of the other two regions (Figure 3c). Unlike the Regions I and II, no zonal propagation of freshwater signal is observed (Figure 4g), suggesting a response to surface freshwater flux changes. Overall, the Aquarius-derived SSS agrees well with the model output for all regions, while the Argo SSS shows relatively weaker amplitudes in Regions I and III. In particular, the Argo SSS in Region I is less than 2 times the seasonal amplitude of the Aquarius. Meanwhile, for Region II, the Argo and Aquarius agree well each other and are close to our model result, showing a strong seasonal variability (see Figures 3 and 4).

The above comparisons reveal a remarkable seasonal SSS variability in these tropical regions and difference and/or agreement among the three different salinity data sets. We here need to discuss why the Aquarius data differ/agree in their annual amplitude from/with the Argo and model. First of all, we can consider the measurement or residual errors in the observations.

The Aquarius v2.0 and lower are known to contain persistent negative salinity bias and seasonal-dependent errors [*Lagerloef et al*., 2013]. The former is related to low-level radio frequency interference from adjacent land areas that will bias the brightness temperatures toward the positive; thus, the salinity will be biased

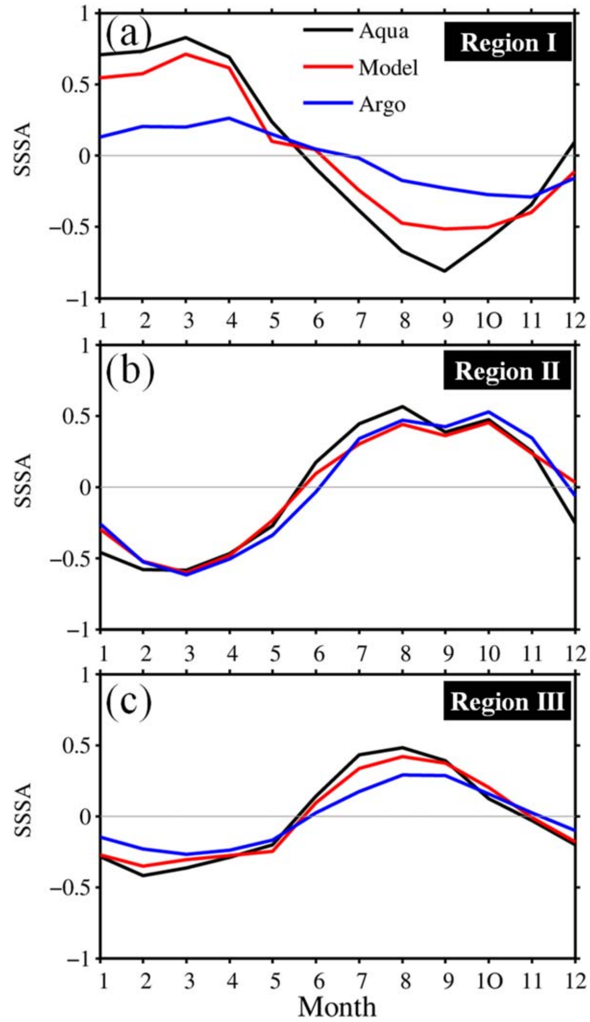

Figure 3. Seasonal cycle of averaged SSS deviations over (a) Region I, (b) Region II, and (c) Region III defined in Figure 1a for Aquarius (black), Argo (blue), and model (red lines) products. All SSS data are monthly averaged for the same month in different years.

negative. The latter is likely related to residual errors in correction for galactic reflection. These errors may be significant in the North Atlantic, Asia-Pacific regions, and at high latitudes, but are relatively small in the topical regions of interest to this study [*Lagerloef*, 2013]. Moreover, these biases were already resolved in the version 2.5 and higher. Recently, an updated Aquarius Combined Active-Passive (CAP) version, which includes galactic correction, Faraday rotation, Antenna Pattern Correction, and minimization of rain effect [*Tang et al*., 2013], improved the accuracy of CAP's salinity [*Yueh*, 2013; *Yueh et al*., 2014]. We compared the Aquarius SSS with the CAP version to estimate the impact of above biases on the study regions, showing a small difference less than 0.1 psu in most regions that cannot explain the differences in the seasonal magnitude between the Aquarius and Argo.

Unlike the Aquarius, the Argo measurements are relatively sparse and have been heavily smoothed that is ineffective particularly for the coastal regions because of its spatial resolution. *Boutin et al*. [2013] suggested that significant difference between SMOS and Argo in the coastal region with the Amazon plume is likely due to the smoothing of Argo data. It seems that the smoothing may largely influence the weakening of SSS variability in comparison with Aquarius and model. However, the Argo data are quite consistent in their annual amplitude with the Aquarius and model output in Region II, and we also minimized the impact near coastal areas by selecting the three open ocean regions far away from the coasts. In addition, the model output is fairly consistent with the Aquarius for all regions, likely suggesting regional responses to dynamical forces rather than artificial biases of Argo like the smoothing. The different regional responses may give us a possible interpretation for the differences/agreements among the different data sets, so we will discuss regionally different dynamics in the next section.

5. Discussions

5.1. Regional Dynamics

Seasonal SSS changes can be largely affected by horizontal salt fluxes and air-sea fluxes (i.e., P and E). Ocean models can simulate these dynamic features. Here we use our model solutions to explain the dynamic cause of those salinity differences/agreements among the salinity data sets. Figure 5 shows the SSS deviations from the annual mean values and surface current from the model result in winter (January to March) and summer (July to September).

In Region I, a positive SSS deviation dominates over the western tropical regions in wintertime when the discharge of Amazon is at its minimum (Figure 5a). During spring to summer when the discharge is

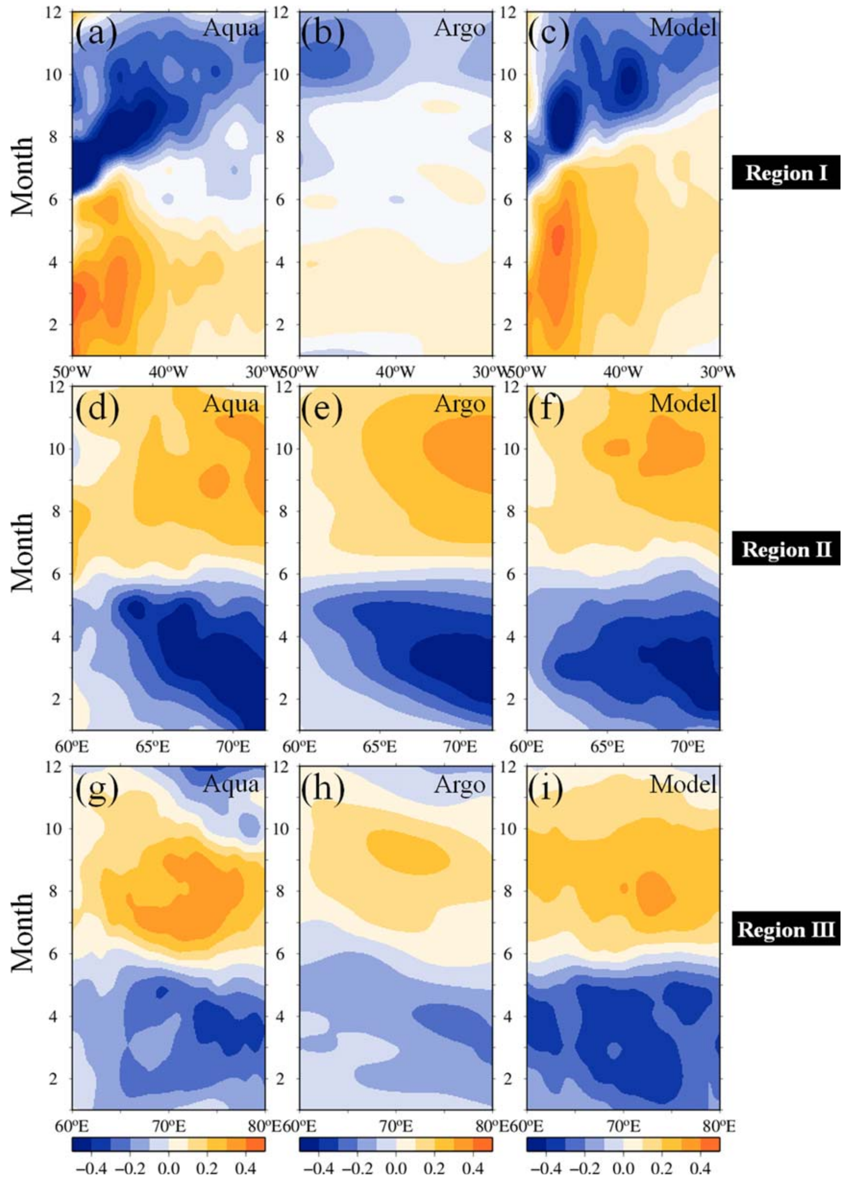

Figure 4. Time-longitude diagrams of SSS deviations in (top) Region I, (middle) Region II, and (bottom) Region III for three SSS products of Aquarius, Argo, and model. All SSS data are monthly averaged for the same month in different years.

substantially increased, on the other hand, the freshwater from the river moves to the north along the northwestward coastal NBC, and is then transported to the east along the NECC around 8°N (Figure 5c). For Region II, it has a strong negative SSS deviation in winter with a westward surface current, while it shows an opposite patterns in summer (Figures 5b and 5d). The seasonal reversal with a westward SSS flux during wintertime and an eastward flux during summertime is due to seasonally reversing monsoon winds in the northern Indian Ocean [*Rao and Sivakumar*, 2003; *Subrahmanyam et al.*, 2011]. Meanwhile, Region III has a strong seasonal SSS variation, but the salt flux is westward year round with weak seasonal changes in its strength (Figures 5b and 5d). It is unlikely that the wind-induced seasonal salt transport plays a critical role in the seasonal SSS variability in Region III.

The freshening in Region I almost corresponds to the highest discharge of the Amazon lagging by about 1–3 months as shown in green line of Figure 6, which shows the climatological river discharge obtained from *Dai et al*. [2009]. The discharge of Amazon reaches its maximum of about 9×10^3 km^3 yr^{-1} during May to June and minimum of about 4×10^3 km^3 yr^{-1} during November to December. The SSS change in this region is also expected to be influenced by the variations of P and E associated with the ITCZ [*Reverdin et al.*,

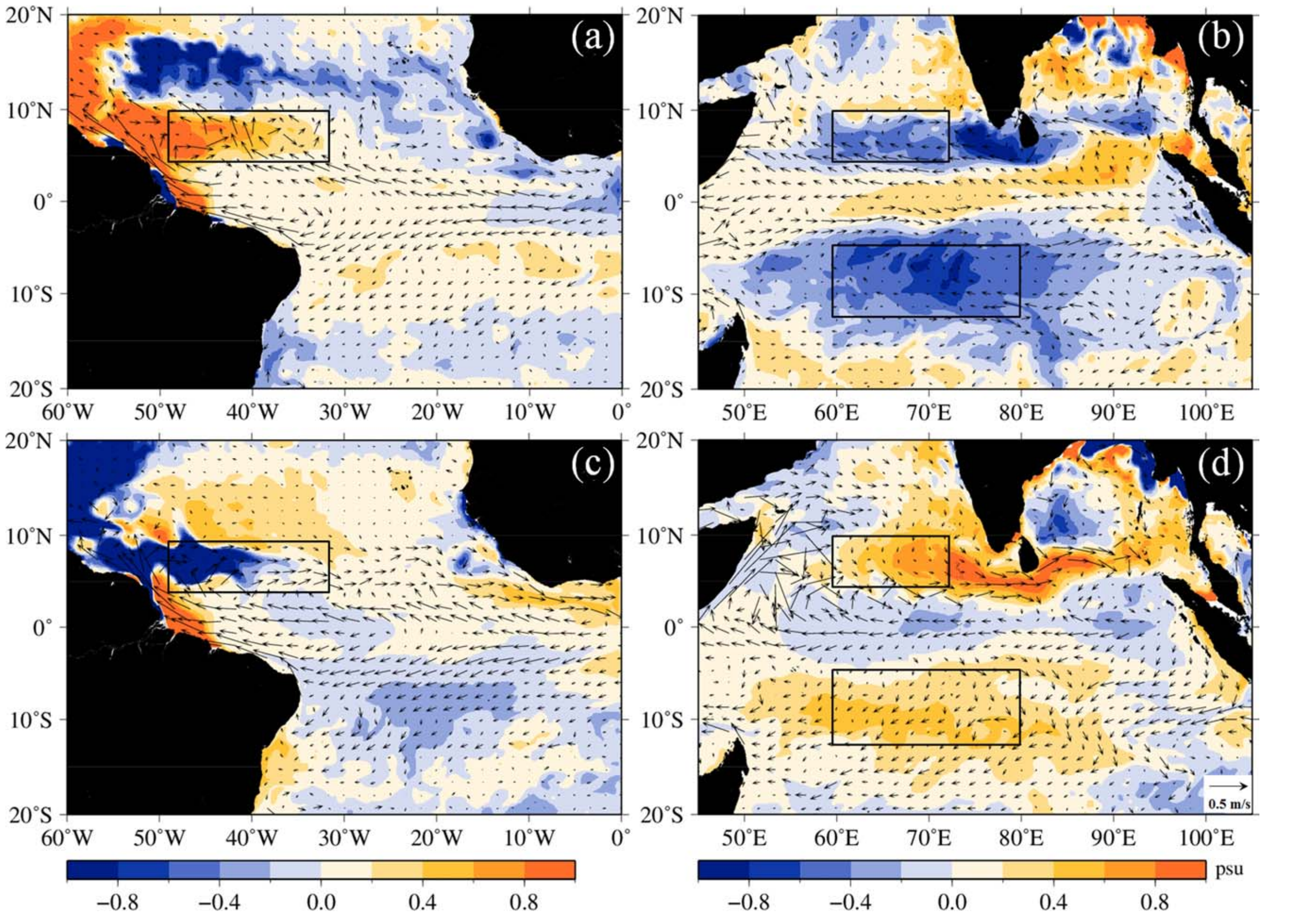

Figure 5. The SSS deviations and surface current from model result for Atlantic Ocean and Indian Ocean during (a and b) wintertime (January to March) and (c and d) summertime (July to September). The boxes indicate the three regions defined in Figure 1a.

2007; *Foltz and McPhaden*, 2008]. To investigate the relationship between the SSS and freshwater fluxes, seasonal cycles of E-P obtained from the NCEP, GPCP, and OAFlux in Region I are shown in blue lines of Figure 6. The values for E and P are obtained by integrating over the Region I to directly compare with the discharge of Amazon [*Tzortzi et al.*, 2013]. It should be noted that because the cycle of E is relatively constant throughout the year (not shown), the seasonal cycle of E-P largely determined by the variability of P rate. The high positive SSS deviations during winter-spring occur when the E-P rate is at a maximum of about 3×10^3 km^3 yr^{-1} during January to February, while it falls during summer-fall when the E-P is close to the minimum (about -1×10^3 km^3 yr^{-1}) of the year. However, the annual cycle of E-P is smaller in magnitude (range from -1×10^3 to 2×10^3 km^3 yr^{-1}) than the river discharge (range from 4×10^3 to 9×10^3 km^3 yr^{-1}; Figure 6), and the strong amplitude mainly lies in the central tropical region rather than in the western part (see Figure 7a), implying more significant role for river discharge in this region. Looking at the amplitude of E-P (Figure 7b), while the annual cycle of E-P shows a weak variability in Region II, there is a high E-P variability in Region III, coincident with the ITCZ, with its minimum in winter and maximum in summer. The P and E fields from NCEP also agree well with the GPCP P and OAFlux E data (now shown), indicating a close relationship between the E-P field and SSS variability in Region III at seasonal time scale [*Bingham et al.*, 2012].

The dynamical difference associated with the salinity changes in the near-surface is evident in Figure 8 that shows the salt budget averaged over the regions. The balance of salt budget is as follows,

$$\frac{\partial S}{\partial t} = -U\frac{\partial S}{\partial x} - V\frac{\partial S}{\partial y} + \frac{(E-P)S}{h} + Q_{dif} \; + H_{dif} \tag{1}$$

where *S* is salinity, *U* and *V* the zonal and meridional component of velocity, and *h* the depth of the upper mixed layer (the model surface layer is used because this work focuses on the near-surface salinity

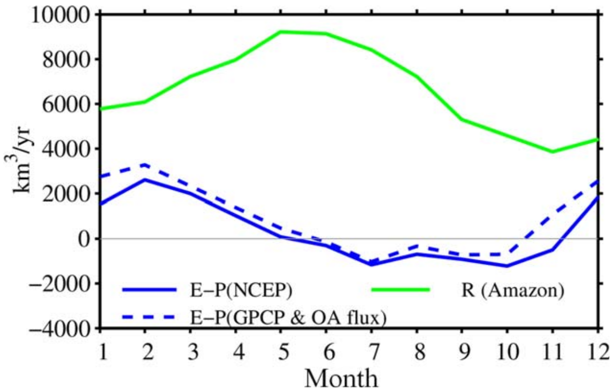

Figure 6. Mean annual cycle of Amazon River discharge (green line) during 1948–2004 obtained from *Dai et al*. [2009], and integrated evaporation (E) minus precipitation (P) over Region I data from NCEP (thick blue), GPCP, and OAFlux data (dashed blue).

processes, which is identified from the differences/agreements among the three salinity data sets). Vertical advection is usually not considered because the mixed layer salinity is assumed to be uniform as that of near-surface salinity. The terms in (1) are the salt tendency (left-hand side), horizontal advection (first and second terms of right-hand side), surface salt flux (third term of right-hand side), vertical (fourth term) and horizontal (fifth term of right-hand side) diffusions. We examined particularly the first three terms of equation, zonal and meridional advection and surface forcing, because the others contribute little to the salt tendency. For Region I (Figure 8a), the change of salt tendency (St) is in phase with zonal advection (zadv) during summertime and with meridional advection (madv) during wintertime, and they have similar magnitudes indicating that the salt change is almost balanced by horizontal advection by NECC, which transports the surface freshwater from Amazon River to the east [*Dessier and Donguy*, 1994; *Da-Allada et al*., 2013]. The freshwater flux also contributes to the SSS changes, but has relatively small effect. This result is consistent with the result of *Grodsky et al*. [2014b], who focused on the local salinity maximum in the northwestern tropical Atlantic. The Region II is also dominated by the annual cycle of SSS (Figure 8b). The period of salt tendency occurs in phase with zonal advection by monthly current, while it varies out of phase with surface freshwater flux (ssfx). This confirms that the salt tendency and horizontal advection almost balance each other, suggesting that seasonal salinity change in this region is dominated by horizontal salt transport by the strong current system due to seasonally reversing monsoon winds in the northern Indian Ocean [e.g., *Rao and Sivakumar*, 2003]. For Region III, on the other hand, the period of salt tendency varies in line with the surface freshwater flux, with a similar magnitude each other (Figure 8c). It is shown that the annual change of SSS is almost balanced by the E-P variability rather than the ocean current in the southern tropical Indian, which has been noted by *Bingham et al*. [2012].

5.2. Vertical Salinity Stratification

Our analysis showed that a large amount of river runoff and/or surface freshwater significantly affects the surface salinity variability in Regions I and III, while the seasonal SSS variability in Region II is closely

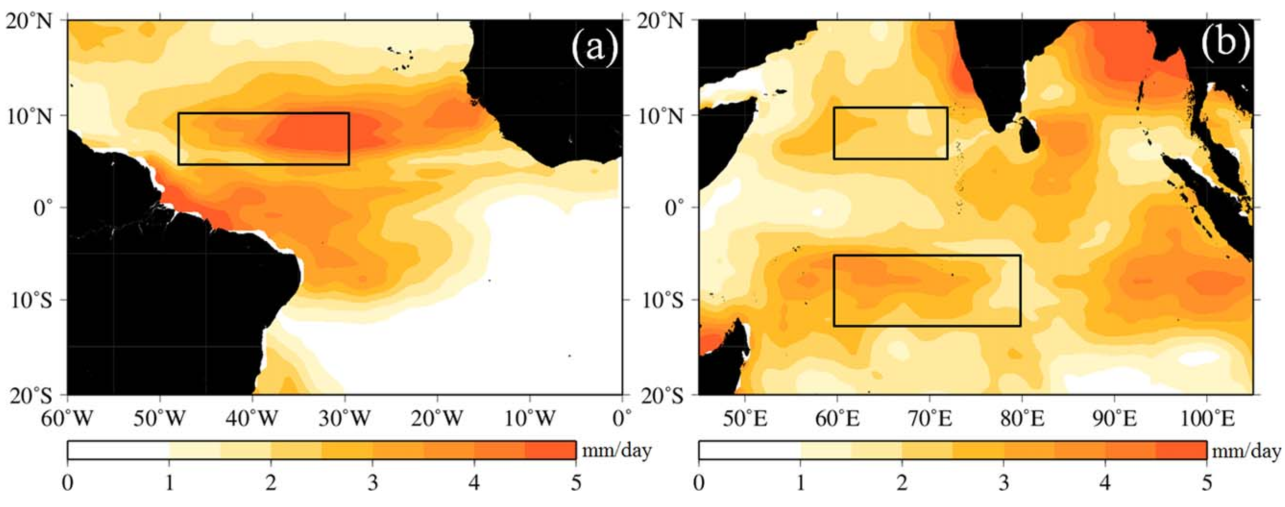

Figure 7. Annual amplitude maps of evaporation (E) minus precipitation (P) from GPCP and OAFlux data in (a) Atlantic Ocean and (b) Indian Ocean. The boxes indicate the three regions defined in Figure 1a.

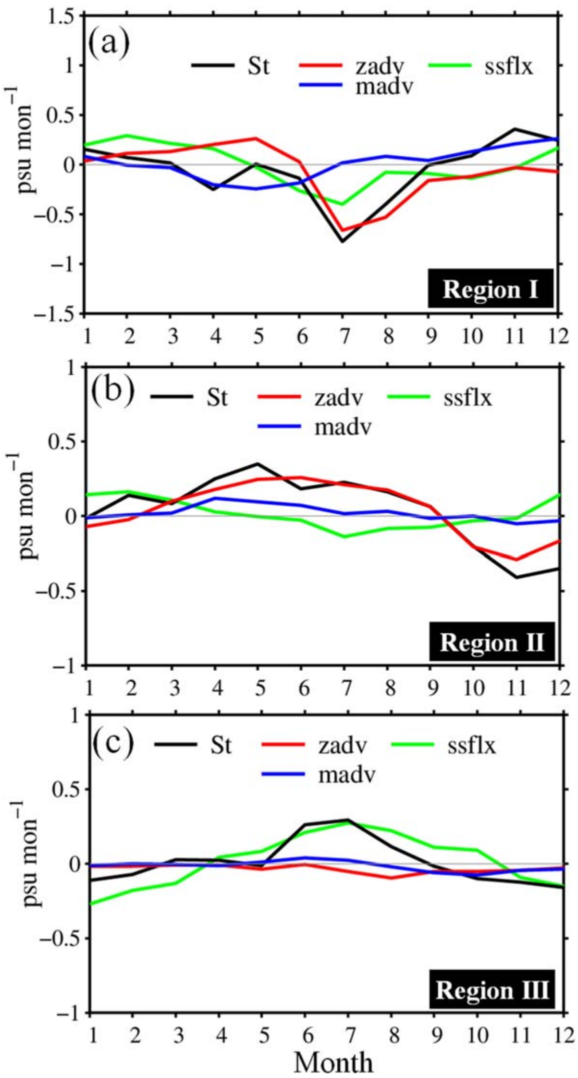

Figure 8. Seasonal cycle of the salt balance between the salinity tendency (black), zonal (red), meridional (blue) advection, and surface freshwater flux (green lines) in (a) Region I, (b) Region II, and (c) Region III.

associated with the salt redistributions due to seasonally reversing ocean current driven by monsoon wind. These different dynamic processes at the surface layer among the three regions are also evident in Figure 9, which compares vertical profiles of seasonal salinity differences for Argo and model, as well as the Aquarius-derived seasonal SSS.

It can be seen that in Region II, the Argo and model profiles agree well each other and also close to the Aquarius at the near-surface. This result in the southern AS suggests that the water at surface layer is seasonally well mixed down to approximately 20 m depth (Figure 9b), showing an agreement between three different salinity products. For Regions I and III, on the other hand, the SSS between the Aquarius and Argo products is significantly different and the water from surface to 20 m depth is relatively stratified compared to the Region II. It emphasizes the effect of changing freshwater at the surface layer associated with the river runoff and/or P variations, resulting in the differences between the two observations and model. In addition, the difference in the subsurface (below 20 m depth) between the Argo and model is relatively small for all regions, showing the model capacity to reproduce the observed salinity profiles in the subsurface layer.

It is worthy of noting that the salinity difference at the surface layer between the different products suggests a signature of the vertical salinity stratification between the top few cm by Aquarius and the 5 m depth by Argo measurements. Our result shows a major contribution of large river discharge to the surface salinity stratification, particularly in the western tropical Atlantic (Region I), where the surface freshwater from Amazon River is transported eastward along the NECC. The impact of rain variability associated with the ITCZ in the southern tropical Indian (Region III) is also consistent with the results of SMOS-derived SSS by *Boutin et al*. [2013] who have recently shown the vertical salinity stratification between the 1 cm and the 5 m depth in rainy regions, comparing the SMOS and Argo measurements. It is shown that in the tropical regions, the river runoff and air-sea exchange of freshwater significantly stratify the sea surface layer above 5 m depth, i.e., Regions I and III. On the other hand, the water can be mixed down to the depth of 5 m in the southern Arabian Sea (Region II), where salinity redistribution occurs due to seasonally reversing ocean currents system, maintaining an agreement among the products. These different dynamic processes have been also confirmed in our model. In Regions I and III, model-predicted SSS values lie between those from Aquarius and Argo, indicating that river discharge and precipitation contribute to the near-surface salinity stratification. In Region II, the model result shows a good agreement with both Aquarius and Argo observations, reproducing the vertical salinity profile due to ocean dynamics (i.e., seasonally reversing ocean currents). These comparisons suggest that the dynamical differences among the three regions can lead to their different vertical salinity stratifications, which explain the Aquarius observations

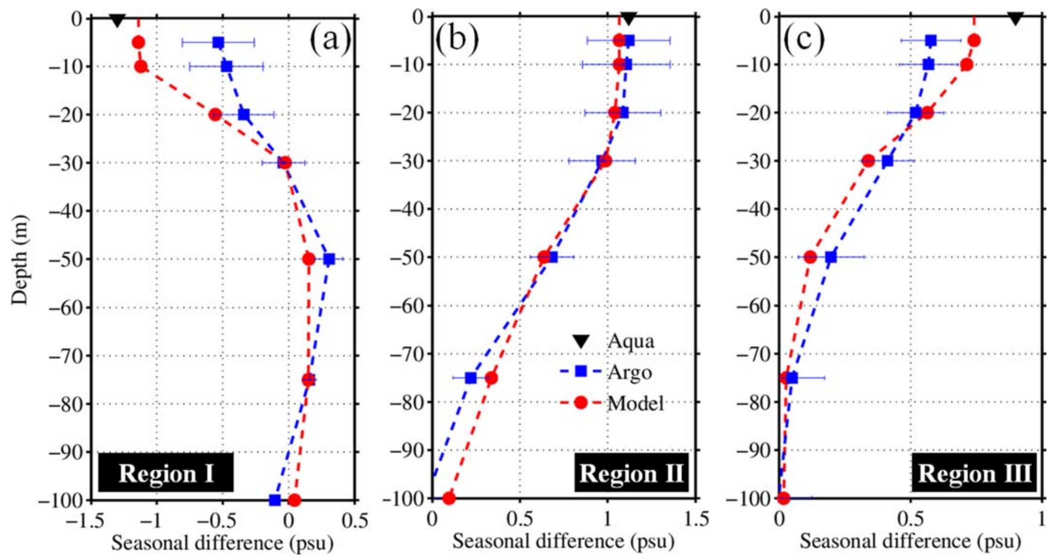

Figure 9. Averaged vertical profiles of seasonal salinity differences between the winter and summer in (a) Region I—a case of stratified by precipitation (P) and river discharge from Amazon, (b) Region II—a case of well mixed, and (c) Region III—a case of stratified by P. The black, blue, and red marks represent for the Aquarius, Argo, and model products, respectively. Also shown are the error bars for Argo product. Notice their different near-surface stratifications and dynamical origins.

in the first cm of the sea surface, and the Argo measurements at the 5 m depth while the model represents the surface layer averaged salinity.

6. Summary

Most of previous studies have focused on comparing satellite SSS measurements from SMOS or Aquarius with Argo data. For a better understanding of the dynamic processes causing their differences, we have used an ocean model to represent the dynamic processes that could not be obtained from data alone. For this purpose, our analysis has been focused on the gridded data products, with a further focus on the averages over the three large regions. We first characterized seasonal SSS variability in the tropical Atlantic/Indian oceans as a case study. We compared the Aquarius SSS with Argo data and ocean model output and examined the dominant processes through analyzing model output as well as the GPCP P and OAflux E data. We then discussed why the Aquarius data differ/agree in their annual amplitude from/with the Argo and model, emphasizing different regional dynamics in each region.

The SSS in the western part of tropical Atlantic (Region I) shows a strong seasonal variability with its maximum in March and minimum in September. The freshening in summer almost corresponds to the highest discharge of the Amazon River. In addition, high SSS deviations during the wintertime occur when the P rate is close to the minimum of the year, while it falls during the summertime when the P is at a maximum, suggesting a relationship between the SSS, river discharge, and P. Meanwhile, for the tropical Indian Ocean, the most dominant feature is zonal band structures of strong SSS variability in the southern AS (Region II) and the southern tropical region (Region III), with negative anomaly in winter and positive anomaly in summer. It is shown that the strong seasonality for the southern AS is mainly caused by the redistribution of SSS due to well-mixed ocean currents, which undergo seasonal reversal due to monsoon wind [e.g., *Rao and Sivakumar*, 2003]. On the other hand, for the southern tropical region, the SSS varies with the annual cycle of P, suggesting a response to changes in surface freshwater flux.

Through the comparisons among the three gridded salinity products, we may suggest that the dynamical differences can lead to their different vertical salinity stratifications locally between the top few cm by Aquarius and the 5 m depth by Argo measurements. In the tropical Atlantic/Indian Oceans, *it is shown* that the large amount of river runoff and air-sea exchange of freshwater significantly stratify the sea surface layer above 5 m depth, which cause the differences between the top few cm by Aquarius and the 5 m depth by Argo (i.e., Regions I and III). On the other hand, the water can be mixed down to the depth of 5 m in the region where the salinity redistribution occurs due to seasonally reversing well-mixed ocean currents system, showing an agreement between the Aquarius and Argo (i.e., Region II).

The results presented here suggest that Aquarius can observe regional SSS variability at seasonal time scale at the top few cm, complement to the traditional Argo near-surface (~5 m depth) measurements, especially in the regions where air-sea freshwater exchange and river runoff dominant [e.g., *Boutin et al.*, 2013]. With further improving their accuracy in the future, Aquarius SSS data would be greatly welcomed by ocean scientists for better understanding of SSS variability on both global and regional scales as well as for assimilating global surface salinity data into ocean models. In addition, the satellite-derived SSS products plus the Argo measurements provide full information about the strong salinity stratification in the ocean surface, which contributes to understanding of air-sea interaction processes like Hurricane-induced mixed layer dynamics [*Grodsky et al.*, 2012].

Acknowledgments
This research is carried out at the Jet Propulsion Laboratory, California Institute of Technology, under contract with the National Aeronautics and Space Administration (NASA). We thank Tangdong Qu for providing the gridded Argo data. The river inflow data have been obtained from www.cgd.ucar.edu/cas/catalog/surface/dai-runoff/index.html, the OAFlux data from http://oaflux.whoi.edu/data.html, and the GPCP data from http://precip.gsfc.nasa.gov/gpcp_v2.2_data.html.

References

Bingham, F. M., G. R. Foltz, and M. J. McPhaden (2012), Characteristics of the seasonal cycle of surface layer salinity in the global ocean, *Ocean Sci.*, *8*, 915–929, doi:10.5194/os-8-915-2012.

Boutin, J., N. Martin, G. Reverdin, X. Yin, and F. Gaillard (2013), Sea surface freshening inferred from SMOS and ARGO salinity: Impact of rain, *Ocean Sci.*, *9*, 183–192, doi:10.5194/os-9-183-2013.

Budgell, W. P. (2005), Numerical simulation of ice-ocean variability in the Barents Sea region, *Ocean Dyn.*, *55*, 370–387, doi:10.1007/s10236-005-0008-3.

Da-Allada , C. Y., G. Alory, Y. du Penhoat, E. Kestenare, F. Durand, and N. M. Hounkonnou (2013), Seasonal mixed-layer salinity balance in the tropical Atlantic Ocean: Mean state and seasonal cycle, *J. Geophys. Res.*, *118*, 332–345, doi:10.1029/2012JC008357.

Dai, A., T. Qian, K. E. Trenberth, and J. D. Milliman (2009), Changes in continental freshwater discharge from 1948–2004, *J. Clim.*, *22*, 2773–2791.

Delcroix, T., M. McPhaden, A. Dessier, and Y. Gouriou (2005), Time and space scales for sea surface salinity in the Tropical oceans, *Deep Sea Res., Part I*, *52*, 787–813.

Dessier, A., and J. R. Donguy (1994), The sea surface salinity in the tropical Atlantic between 10S and 30N seasonal and interannual variations (1977–1989), *Deep Sea Res., Part I*, *41*, 81–100.

Donguy, J. E., and G. Meyers (1996), Seasonal variations of sea surface salinity and temperature in the tropical Indian Ocean, *Deep Sea Res., Part I*, *43*, 117–138.

Fairall, C. W., E. F. Bradley, D. P. Rogers, J. B. Edson, and G. S. Young (1996), Bulk parameterization of air-sea fluxes for tropical ocean-global atmosphere coupled-ocean atmosphere response experiment, *J. Geophys. Res.*, *101*, 3747–3764, doi:10.1029/95JC03205.

Foltz, G. R., and M. J. McPhaden (2008), Seasonal mixed layer salinity balance of the tropical North Atlantic Ocean, *J. Geophys. Res.*, *113*, C02013, doi:10.1029/2007JC004178.

Grodsky, S. A., N. Reul, G. Lagerloef, G. Reverdin, J. A. Carton, B. Chapron, Y. Quilfen, V. A. Kudryavtsev, and H.-Y. Kao (2012), Haline hurricane wake in the Amazon/Orinoco plume: AQUARIUS/SACD and SMOS observations, *Geophys. Res. Lett.*, *39*, L20603, doi:10.1029/2012GL053335.

Grodsky, S. A., G. Reverdin, J. A. Carton, and V. J. Coles (2014a), Year-to-year salinity changes in the Amazon plume: Contrasting 2011 and 2012 Aquarius/SACD and SMOS satellite data, *Remote Sens. Environ.*, *140*, 12–22, doi:10.1016/j.rse.2013.08.033.

Grodsky, S. A., J. A. Carton, and F. O. Bryan (2014b), A curious local surface salinity maximum in the northwestern tropical Atlantic, *J. Geophys. Res. Oceans*, *119*, 484–495, doi:10.1002/2013JC009450.

Henocq, C., J. Boutin, G. Reverdin, F. Petitcolin, S. Arnault, and P. Lattes (2010), Vertical variability of near-surface salinity in the tropics: Consequences for L-band radiometer calibration and validation, *J. Atmos. Oceanic Technol.*, *27*, 192–209, doi:10.1175/2009JTECHO670.1.

Hu, C., E. T. Montgomery, R. W. Schmitt, and F. E. Muller-Larger (2004), The dispersal of the Amazon and Orinoco River water in the tropical Atlantic and Caribbean Sea: Observation from space and S-PALACE floats, *Deep Sea Res., Part II*, *51*, 1151–1171.

Huffman, G. J., and D. T. Bolvin (2012), *GPCP Version 2.2. Combined Precipitation Data Set Documentation*, Lab. for Atmos., Natl. Aeronaut. and Space Admin., Washington, D. C. [Available at ftp://precip.gsfc.nasa.gov/pub/gpcp-v2.2/doc/V2.2_doc.pdf.]

Kalnay, E., et al. (1996), The NCEP/NCAR, 40-year reanalysis project, *Bull. Am. Meteorol. Soc.*, *77*(3), 437–471.

Lagerloef, G., et al. (2008), The Aquarius/SAC-D mission: Designed to meet the salinity remote-sensing challenge, *Oceanography*, *21*, 68–81.

Lagerloef, G., et al. (2013), Aquarius salinity validation analysis: Data version 2.0, Aquarius Proj. Doc. AQ-014-PS-0016, 36 pp. [Available at http://aquarius.nasa.gov/pdfs/AQ-014-PS-0016_AquariusSalinityDataValidationAnalysis_DatasetVersion2.0.pdf.]

Nikiemaa, O., J.-L. Devenon, and M. Baklouti (2007), Numerical modeling of the Amazon River plume, *Cont. Shelf Res.*, *27*, 873–899.

Nyadjro, E. S., B. Subrahmanyam, V. S. N. Murty, and J. F. Shriver (2010), Salt transport in the near-surface layer in the monsoon-influenced Indian Ocean using HYCOM, *Geophys. Res. Lett.*, *37*, L15603, doi:10.1029/2010GL044127.

Qu, T., Y. T. Song, and C. Maes (2014), Sea surface salinity and barrier layer variability in the equatorial Pacific as seen from Aquarius and Argo, *J. Geophys. Res. Oceans*, *119*, 15–29, doi:10.1002/2013JC009375.

Rao, R. R., and R. Sivakumar (2003), Seasonal variability of sea surface salinity and salt budget of the mixed layer of the north Indian Ocean, *J. Geophys. Res.*, *180*(C1), 3009, doi:10.1029/2001JC000907.

Ravichandran, M., P. M. Vinayachandran, S. Joseph, and K. Radhakrishnan (2004), Results from the first Argo float deployed by India, *Curr. Sci.*, *86*, 651–659.

Reverdin, G., E. Kestenare, C. Frankignoul, and T. Delcroix (2007), Surface salinity in the Atlantic Ocean (30_S–50_N), *Prog. Oceanogr.*, *73*, 311–340, doi:10.1016/j.pocean.2006.11.004.

Roemmich, D., and J. Gilson (2009), The 2004–2008 mean and annual cycle of temperature, salinity and steric height in the global ocean from Argo Program, *Prog. Oceanogr.*, *82*, 81–100, doi:10.1016/j.pocean.2009.03.004.

Schott, F., and J. P. McCreary (2001), The monsoon circulation of the Indian Ocean, *Prog. Oceanogr.*, *51*, 1–123.

Shchepetkin, A., and J. C. McWilliams (2005), The regional oceanic modeling system (ROMS): A split-explicit, free-surface, topography-following coordinate oceanic model, *Ocean Modell.*, *9*, 347–404, doi:10.1016/j.ocemod.2004.08.002.

Song, Y., and D. Haidvogel (1994), A semi-implicit primitive equation ocean circulation model using a generalized topography-following coordinate system, *J. Comput. Phys.*, *115*, 228–244, doi:10.1006/jcph.1994.1189.

Song, Y. T., and T. Y. Hou (2006), Parametric vertical coordinate formulation for multiscale, Boussinesq, and non-Boussinesq ocean modeling, *Ocean Modell.*, *11*, 298–332, doi:10.1016/j.ocemod.2005.01.001.

Subrahmanyam, B., V. S. N. Murty, and D. M. Heffner (2011), Sea surface salinity variability in the tropical Indian Ocean, *Remote Sens. Environ.*, *113*, 944–956.

Subrahmanyam, B., G. Grunseich, and E. S. Nyadjro (2012), Preliminary SMOS salinity measurements and validation in the Indian Ocean, *IEEE Trans. Geosci. Remote Sens.*, *51*, 19–27.

Tang, W., S. Yueh, A. Fore, G. Newmann, A. Hayashi, and G. Lagerloef (2013), The rain effect on Aquarius' L-band sea surface brightness temperature and radar backscatter, *Remote Sens. Environ.*, *137*, 147–157.

Tzortzi, E., S. A. Josey, M. Srokosz, and C. Gommenginger (2013), Tropical Atlantic salinity variability: New insights from SMOS, *Geophys. Res. Lett.*, *40*, 2143–2147, doi:10.1002/grl.50225.

Yu, L. (2011), A global relationship between the ocean water cycle and near-surface salinity, *J. Geophys. Res.*, *116*, C10025, doi:10.1029/2010JC006937.

Yu, L., X. Jin, and R. A. Weller (2008), Multidecade global flux datasets from the objectively analyzed air-sea fluxes (OAFlux) project: Latent and sensible heat fluxes, ocean evaporation, and related surface meteorological variables, *Tech. Rep. OA2008-01*, Woods Hole Oceanogr. Inst., Woods Hole, Mass. [Available at http://oaflux.whoi.edu/publications.html.]

Yueh, S. (2013), Aquarius CAP algorithm and data user guide, JPL report, pp. 20, Jet Propul. Lab., Pasadena, Calif. [Available at http://podaac.jpl.nasa.gov/aquarius/.]

Yueh, S., W. Tang, A. Fore, A. Hayashi, Y. T. Song, and G. Lagerloef (2014), Aquarius geophysical model function and combined active passive algorithm for ocean surface salinity and wind retrieval, *J. Geophys. Res. Oceans*, *119*, doi:10.1002/2014JC009939.